Cambridge Materials: Energy (2026), **1**, e1, 1–15
doi:10.1017/S2978169826000008

CAMBRIDGE UNIVERSITY PRESS

Review

Atomic defect engineering in tungsten oxide photocatalysts

Min Shen[1], Sikang Xue[2], Xuefeng Lu[1], Sibo Wang[1], Jinshui Zhang[1], Zhiyang Yu[1] and Can Yang[1]

[1]The State Key Laboratory of Photocatalysis on Energy and Environment, College of Chemistry, Fuzhou University, Fuzhou, China and [2]State Key Laboratory of Opto-Electronic Information Acquisition and Protection Technology, Leibniz International Joint Research Center of Materials Sciences of Anhui Province, Institutes of Physical Science and Information Technology, Anhui University, Hefei, China

Abstract

Defect engineering is a widely used strategy for tailoring the band structures and surface-active sites of tungsten trioxides (WO_3) nanomaterials, thereby enhancing their photocatalytic performance. In particular, precise control of defect topology is recognized as a pivotal step in constructing surface-active sites, enabling the regulation of surface atomic configurations through the deliberate design of defect types and their terminations. This mini-review elucidates the roles of various surface defect types of WO_3 semiconductors in photocatalytic redox reactions, revealing how surface defect topology activates reactants at the atomic level. It aims to provide insightful information on defective photocatalysts to guide the optimization of the electronic structures inside photocatalysts, thereby establishing a computational-experimental framework for next-generation adaptive photocatalyst architectures.

Impact Statement

Developing highly efficient photocatalysts through defect engineering is of great significance for solar energy conversion, carbon neutrality, and environmental sustainability. Although extensive studies have explored defect-mediated photocatalysis, a unified understanding of the atomic-scale mechanisms governing photocatalytic CO_2 reduction and related reactions remains elusive due to the complexity of charge transfer and surface reaction pathways. In this mini-review, we systematically summarize recent advances in atomic defect engineering of WO_3-based photocatalysts, with particular emphasis on the atomic-scale origins of defect-induced catalytic activity. We discuss how various defect configurations, including oxygen vacancies, tungsten vacancies, disordered lattices, and ordered line defects, modulate the local electronic structures, surface coordination environments, and interfacial charge-transfer dynamics of WO_3 photocatalysts. Special attention is devoted to correlating defect-induced electronic reconstruction with molecular adsorption/activation behaviors and reaction selectivity in photocatalytic CO_2 reduction, water oxidation, H_2O_2 production, and selective organic transformations. Furthermore, advanced atomic-resolution characterization techniques and theoretical simulations are used to reveal the dynamic evolution of defect structures under realistic reaction conditions. This review also addresses key challenges toward practical implementation, including controllable defect fabrication, long-term structural stability, and operando identification of active sites. By bridging atomic-scale defect chemistry with photocatalytic functionality, this work provides mechanistic insights and rational design principles for next-generation WO_3 photocatalysts and other defect-engineered semiconductor systems for sustainable solar-to-chemical energy conversion.

Keywords: Atomic structures; Photocatalysis; Polarization activation; Surface defect; Tungsten oxide

(Received: 03 June 2026; revised: 24 July 2026; accepted: 04 August 2026)

1. Introduction

Inspired by the natural photosynthesis strategy, photocatalysis is a promising method to directly store solar energy by forming chemical products [1,2,3]. The photocatalytic processes are divided into three main steps [4,5]: (1) photocatalysts harvest photons to produce photocarriers under irradiation; (2) the separation and migration of photoinduced charge carriers; and (3) surface photogenerated carriers involved in the adsorption and activation of reactants. Unfortunately, pristine photocatalysts exhibit a limited light-absorption range, serious charge recombination, and sluggish surface reaction kinetics for certain molecules (including CO_2 [6], H_2O [7,8], benzene [9], etc. [10,11]), which limits the development of photocatalysis techniques [6]. The defect engineering of semiconductors provides a brand new way to modulate the geometric configurations of photocatalysts to improve photocatalytic conversion efficiency [7,8]. Generally, the types of defects impact the band structures of photocatalysts [9]. Specifically, the surface point defect introduces shallow trap levels to readily capture photogenerated electrons, whereas stacking faults introduce deep defect trap levels within the photocatalysts [10,11]. In addition to narrowing the band gap, the surface defect can introduce surface band bending to enhance charge separation efficiency. Regarding surface reaction kinetics, low-coordination defect sites exhibit two critical catalytic advantages [12]: (1) the asymmetric electron configurations create highly active sites that facilitate orbital hybridization with

Corresponding authors: Zhiyang Yu; Can Yang; Emails: yuzyemlab@fzu.edu.cn; canyang@fzu.edu.cn

Cite this article: M. Shen, S. Xue, X. Lu, S. Wang, J. Zhang, Z. Yu and C. Yang. 'Atomic defect engineering in tungsten oxide photocatalysts'. *Cambridge Materials: Energy*, **1**, e1: (2026), 1–15. https://doi.org/10.1017/S2978169826000008

© The Author(s), 2026. Published by Cambridge University Press. This is an Open Access article, distributed under the terms of the Creative Commons Attribution licence (http://creativecommons.org/licenses/by/4.0), which permits unrestricted re-use, distribution and reproduction, provided the original article is properly cited.

Downloaded from https://www.cambridge.org/core. 18 Nov 2026 at 09:38:25, subject to the Cambridge Core terms of use.

adsorbates [12,13,14]; (2) the lattice distortion near defect regions lowers the activation barrier to facilitate intermediate adsorption/desorption energetics [15]. Thus, the defect engineering of the photocatalysts contributes to improving the photocatalytic reaction efficiency.

Defects in WO_3 can be broadly classified as surface and bulk defects, which play distinct but interconnected roles in photocatalytic processes [16,17]. Surface defects are directly exposed to the reaction environment and primarily regulate molecular adsorption, activation, interfacial charge transfer, and surface reaction pathways [18,19,20]. In contrast, bulk defects mainly influence the electronic structure, carrier trapping, recombination, and transport within the photocatalyst [21,22,23]. Bulk oxygen vacancies may also migrate, aggregate, or terminate at the surface, thereby modifying local surface coordination environments [24]. Among metal oxide photocatalysts, N-type WO_3 materials were first used as a stable semiconductor to promote the photoelectrolysis of water due to their band gap of 2.7 eV in 1976, which was lower than that of TiO_2 photocatalysts (3.2 eV) [25]. Bard et al. then employed WO_3 powders as the photocatalyst to achieve the photoreduction deposition of copper in 1979 [26]. Moreover, carbon dioxide (CO_2) could also be reduced to methanol [27], methane [28], and formaldehyde [29] with the assistance of water vapor and WO_3 photocatalysts under irradiation [29]. To date, WO_3 is still one of the most attractive candidates for photocatalysis [30,31] and photoelectrocatalysis [32] due to its low cost, moderate hole-diffusion length (*ca.* 150 nm) [33], and stable photochemical properties [34]. To improve carrier transport behavior and expose plentiful metal sites, many oxygen-deficient Magnéli-phase oxides (WO_{3-x}, $x < 3$) with different defect types, such as $WO_{2.92}$ [35], $WO_{2.9}$ [36], $WO_{2.83}$ [37], $WO_{2.72}$ [38,39], have been developed [40,41]. It should be noted that defective WO_3 and oxygen-deficient tungsten oxide phases are related but not identical concepts. Defective WO_3 refers to WO_3 containing isolated or low concentrations of oxygen vacancies while largely preserving the parent WO_3 crystal framework [22,42]. As the oxygen vacancy concentration further increases, these vacancies can aggregate and produce high-dimensional and specific defects, leading to the formation of oxygen-deficient tungsten oxide phases (WO_{3-x}, referred to as Magnéli phases, such as $WO_{2.92}$, $WO_{2.9}$, $WO_{2.72}$, and $W_{18}O_{49}$) [24]. These oxygen-deficient phases are discussed in this review because they provide important insights into the evolution of defect structures and the corresponding photocatalytic mechanisms. Oxygen vacancy (V_O) has been the most widely studied in the reported literature [22], which can narrow the bandgap of WO_3 (down to ~2.4 eV), thereby extending visible-light absorption wavelengths beyond 600 nm [41,43]. Meanwhile, the loss of surface oxygen atoms exposed W^{5+} species that facilitate the adsorption and activation of reactants and intermediate species, resulting in a marked improvement in photocatalytic performance, as demonstrated in several studies [44,45]. Other structural defects, such as grain boundaries [46] and dislocations [47] in nanostructured WO_3 (e.g., porous frameworks or nanosheets), provide efficient charge transport pathways and accelerate carrier migration [44,45]. Collectively, these findings demonstrate that the types of defects play vital roles in tailoring the physicochemical properties of nanostructured WO_3 photocatalysts for improving photocatalytic properties [48,49].

In recent years, systematic breakthroughs have been achieved in understanding how surface defect types of WO_3 fundamentally govern the underlying mechanism of photocatalytic processes [50]. However, the understanding of the potential effects of defects with diverse topologies on photocatalytic processes is missing. This mini-review delves into the formation and activation mechanism of diverse defect types in WO_3 photocatalysts and provides the theoretical basis for the rational design of defective photocatalysts. The detailed contents are as follows: (1) elucidating the formation and dynamic evolution mechanisms of various defects types in tungsten oxides; (2) establishing structure–property relationships by resolving how these defect configurations modulate band structures by forming localized states at the atomic scale; (3) providing molecular-level mechanistic insights into how specific defect architectures facilitate reactant adsorption, lower activation barriers, and guide reaction pathways. Finally, we critically analyze persistent challenges in defect engineering, including issues under operational conditions and the difficulties in achieving the precise modulation of defect types.

2. The Phase Structures of Defective Tungsten Trioxides

The crystal structures of WO_3 are composed of the corner-sharing [WO_6] octahedra [51], as shown in Figure 1a, where the centered W atom is bonded with six adjacent O atoms [52]. Given that the corner-sharing [WO_6] octahedra exhibit various tilting and rotation angles under different environments, the phase structures of WO_3 can be divided into tetragonal α-WO_3, orthorhombic β-WO_3, monoclinic γ-WO_3, triclinic δ-WO_3, and monoclinic ε-WO_3 [44,53]. As shown in the phase diagram of the WO_3 sample as a function of temperature in Figure 1b, increasing the temperature from 0 °C under an oxygen-rich environment induces a phase transition from triclinic δ-WO_3 to tetragonal α-WO_3, showing temperature-dependent evolution of the crystal structures [54,55]. With the increased O-W-O bond angles along the [100], [010], and [001] directions, the crystal symmetry of WO_3 improves until it approaches an "ideal" cubic structure [56]. Among these structures, the monoclinic γ-WO_3 is the common and stable phase that exists at room temperature [44,53]. As depicted in Figure 1c, the yellow WO_3 consists of corner-sharing distorted [WO_6] octahedra with a band gap of 2.8 eV, whose band structure positions meet the requirements of overpotentials for some photocatalytic redox reactions [57,58]. However, the apparent quantum yield of the pristine γ-WO_3 photocatalysts is poor compared to the natural photosynthesis reaction efficiency without any cocatalysts and modifications [59,60]. To expand the light absorption in visible light and construct more active sites at the surface, various chemical reduction methods introduced diverse defects within the γ-WO_3 catalysts, including hydrogenation [61,62], liquid-phase reduction [63,64], *etc* [65].

Yellow WO_3 is a typical substoichiometric compound at room temperature, having a certain concentration of V_O in bulk [66,67]. As the concentration of V_O rose in bulk, the substoichiometric ratio between O and W atoms would be lower than 3, forming oxygen-deficient tungsten oxide materials [68]. These defects would produce a defect level in the forbidden band below the conduction band, where the position is dependent on the defect concentrations [69]. Meanwhile, the existence of the V_O in bulk WO_3 produces plentiful dangling bonds to increase the concentrations of photoexcited electrons, resulting in the Burstein–Moss shift [70]. The narrowed band gap and up-shifted Fermi level of the γ-WO_{3-x} crystals contribute to broadening their absorption ranges in visible and infrared light due to the additional defect levels and local surface plasmon resonance (LSPR) [71,72]. When V_O continually rises, it would be gathered and reconstructed to produce well-known Magnéli phases [73], including $WO_{2.92}$, $WO_{2.9}$ (blue tungsten oxide), $WO_{2.72}$ (violet tungsten oxide), $WO_{2.67}$, *etc* [41,51]. As seen in the upper panel

Downloaded from https://www.cambridge.org/core. 18 Nov 2026 at 09:38:25, subject to the Cambridge Core terms of use.

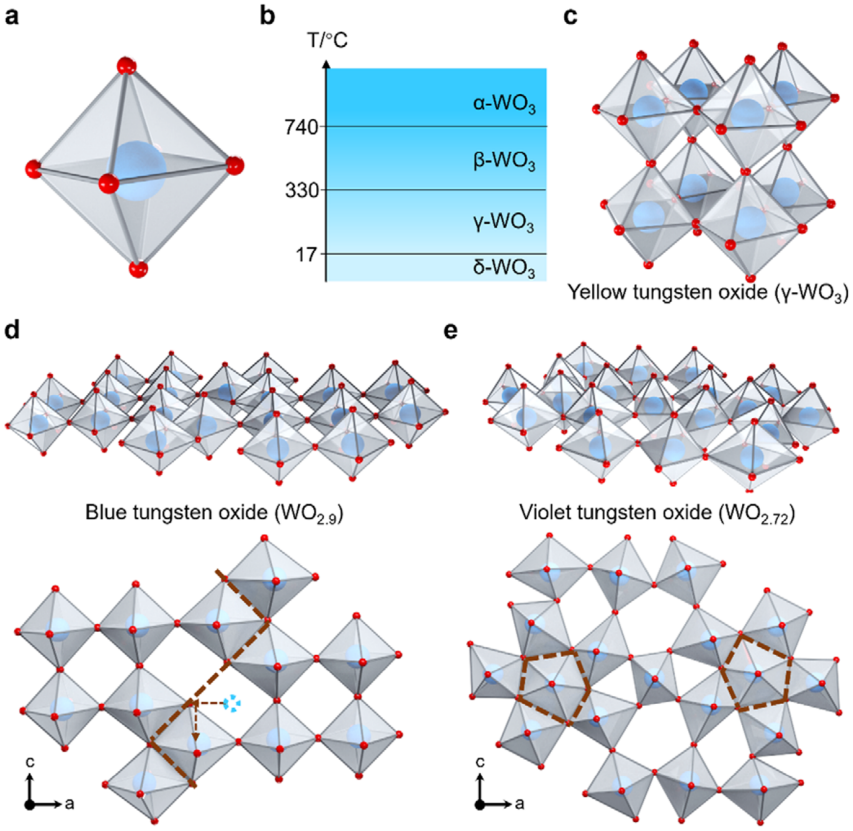


Figure 1. (a) The structural units of [WO_6] octahedra in tungsten oxides. Reproduced with permission of Ref. [52]. Copyright 2006, American Chemical Society. (b) The phase diagram of tungsten trioxides as a function of temperature, with an emphasis on 21 wt% oxygen content (redrawn from Ref. [55]). (c) The atomic structures of the yellow tungsten oxide, which corresponds to the γ-WO_3, consisting of corner-sharing [WO_6] octahedra. (d) The phase structure of (upper panel) the blue tungsten oxide and its atomic configuration (lower panel) along the [010] zone axis [74]. (e) The crystal structures of violet $WO_{2.72}$ (upper panel) and its structures from the top view (lower panel) [75]. The blue and red spheres refer to the W and O atoms, respectively.

of Figure 1d, the crystal structure of the blue tungsten oxide was composed of corner-sharing and edge-sharing [WO_6] octahedra, which is different from $WO_{2.92}$ structures with V_O [66]. From the atomic configuration of the $WO_{2.9}$ phase along [010] direction (the lower panel of Figure 1d), half of [WO_6] octahedra to the right of the dotted brown line have shifted 1/2 distances of O-W-O bond length along the (200) and (002) planes as marked by brown arrows, making corner-sharing connected [WO_6] octahedra changed to edge-sharing connected [WO_6] octahedra, thereby inducing the formation of stacking faults [24,74]. This structure reconstruction is accompanied by the formation of many three-coordinated O atoms to reduce the stoichiometric ratio of tungsten oxides, producing $WO_{2.9}$ Magnéli phases [24].

For $WO_{2.72}$, its phase structures show different polyhedron connection patterns as compared to the blue tungsten oxide in the upper panel of Figure 1e [75]. In the atomic model of the $WO_{2.72}$ phase from the [010] direction, we found that the [WO_6] octahedral structural units show varying degrees of distortion in the bond length and bond angles in the a, b, and c directions that are connected by corner-sharing at the structures [76]. Meanwhile, surrounded [WO_6] octahedra have been tilted and rotated to form edge-sharing connections, producing two [WO_7] decahedra as boxed by brown dashed lines [69]. Due to the distorted structures of the monoclinic $WO_{2.72}$ phase, the $WO_{2.72}$ phase shows metal-like band structures [69]. The edge-sharing connections over [WO_6] octahedra result in delocalized electronic structures, increasing carrier concentration, and thereby improving the electrical conductivity of WO_3 [77,78].

2.1. The Evolution Mechanism of Various Defect Types

Defects originating from the crystal structures that break the periodicity of atom stacking in materials were classified into three types according to their dimensions: point, line, and planar defects [79]. These defects can be generally constructed by employing various reduction methods with specific reaction environments to form Magnéli phases of WO_3 materials, including gas phase reduction [80,81], liquid phase reduction [82], and solid phase reduction [83]. The basic principle of constructing defects is applying the reducibility of reaction agents to seize the lattice oxygen, forming different defect types in various Magnéli phases.

Yu et al. have investigated the dynamic evolution mechanism of defect types with increased temperature under a 5 wt% H_2/Ar atmosphere by employing *in situ* transmission electron microscopy (TEM) [24]. As shown in Figure 2a, hydrogen reduction generates a certain concentration of V_O in WO_3 nanosheets, and their concentration increases positively with the heat treatment temperature. When the temperature reached 350 °C, the V_O would gather to trigger the rotation of [WO_6] octahedra, resulting in the appearance of the {120} stacking faults in a unique zigzag form (Figure 2b). With the temperature increased to 450 °C, we found that the [WO_6]

Downloaded from https://www.cambridge.org/core. 18 Nov 2026 at 09:38:25, subject to the Cambridge Core terms of use.

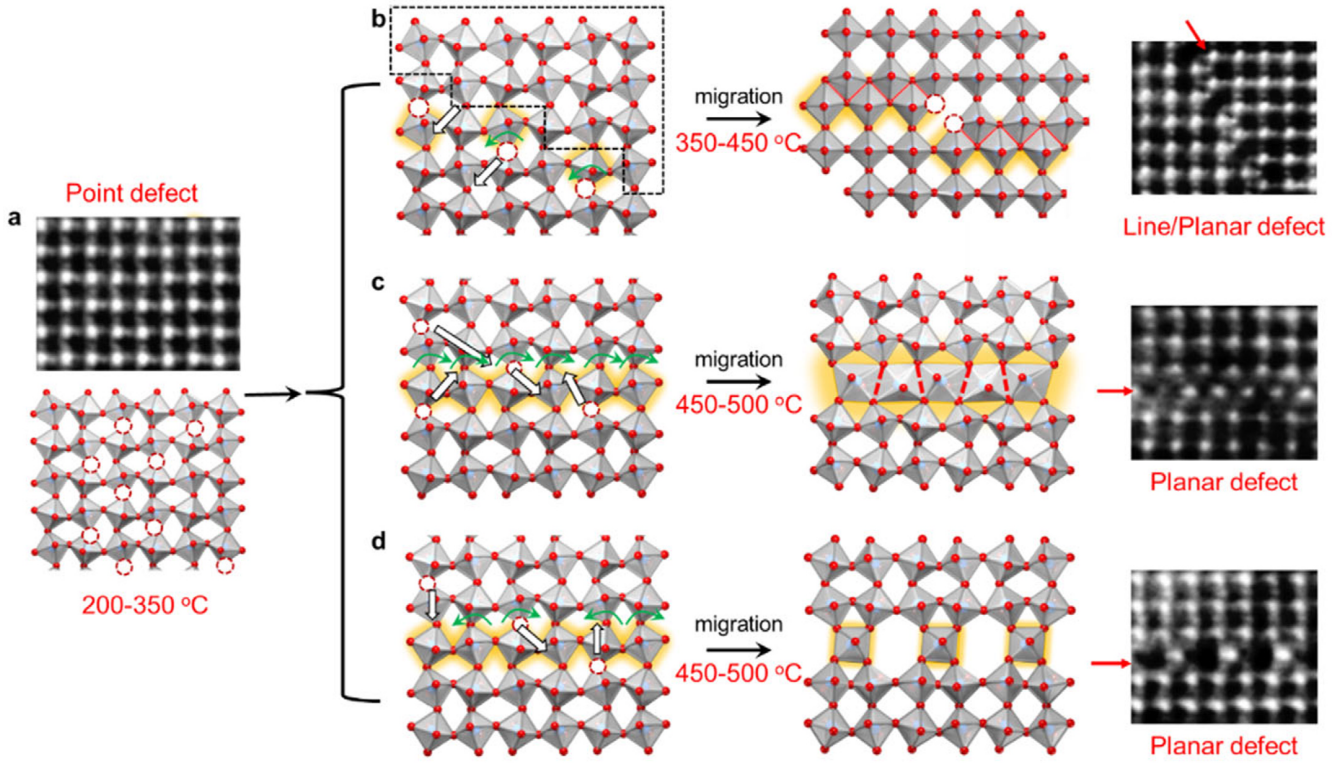


Figure 2. (a–d) The microstructure of the γ-WO_3 crystal at the increased temperature from 200 °C to 500 °C under the 5% H_2/Ar atmosphere. Reproduced with permission of Ref. [24]. Copyright 2021, American Chemical Society.

octahedra have been tilted by 45° to form {200}-1X (Figure 2c) and {200}-2X (Figure 2d) stacking faults along [100] directions. These results indicate that γ-WO_3 materials show temperature-dependent defect types.

Except for the approaches mentioned above, the photochemical reduction method is an effective strategy to obtain abundant V_O defects inside the WO_3 particles. For instance, Wang et al. used photo-excited electrons to reduce the bulk of WO_3 materials for constructing V_O under a solution with electron donors [84]. Meanwhile, multiple-step reduction methods have been employed to optimize the surface atomic structures for changing the selectivity of products [85]. It is worth noting that the influence of defect types on photocatalytic properties is complex, since their terminations on the surface can modulate surface atomic structures and concurrently affect the transport behavior of photogenerated carriers [86].

The crystal surface, defined as the boundary interface terminating periodic atomic arrangements, exhibits various structural imperfections when defects from the bulk material terminate at this surface [87]. These surface defects dependent on their dimensions, can also be categorized into three primary classifications [79]: (1) surface point defects, manifested as adatoms (surface-adsorbed atoms) or vacancies (missing lattice atoms) [88]; (2) surface linear defects, including step edges and kink sites [89]; and (3) surface planar defects [90], typically characterized by atomically rough surfaces with disrupted periodicity.

These types of defects at the surface fundamentally change the local atomic coordination and the surface energy landscape, significantly impacting the material's chemical reactivity and physical properties [91]. Understanding how surface defects drive the adsorption and polarization of molecules is essential. Furthermore, the spatial distribution of these defects is crucial in determining their roles. Bulk defects typically serve as recombination centers for photogenerated carriers, whereas surface defects, rich in dangling bonds, act as active sites that facilitate surface reaction dynamics. The specific roles of these surface defects in photocatalytic processes will be discussed in detail below.

2.2. The Role of the Surface Point Defect

Surface point defects contain surface adatoms [92,93,94], W interstitials [23], W vacancies, and O vacancies [95,96,97]. Among them, surface V_O is the most frequently reported in the literature, since it is easily generated during experiments. The construction of surface V_O causes the exposure of W atoms, acting as a surface-active site for adsorbing the reactants and polarizing the electronic structures of molecules in the WO_3 photocatalyst [98]. Zhou et al. [84] reported that the WO_3-*hv*-1.0 h sample generated abundant V_O on the {002} surface of photocatalysts under irradiation, which effectively enhanced the adsorption of oxygen and the formation of superoxide radicals (Figure 3a–e). What's more, the production of V_O facilitates the spatial separation of photoexcited charge carriers, establishing dual activation pathways to activate benzene under visible light and improve the phenol yield, as shown in Figure 3f,g. However, excessive surface V_O concentration could impair the photocatalytic performance, because the high density of V_O serves as a recombination center for photocarriers. The influence of oxygen vacancies on photocatalytic performance is highly dependent on their concentration [21]. At low to moderate concentrations, oxygen vacancies introduce defect states within the band gap, broaden visible-light absorption, increase carrier density,

Downloaded from https://www.cambridge.org/core. 18 Nov 2026 at 09:38:25, subject to the Cambridge Core terms of use.

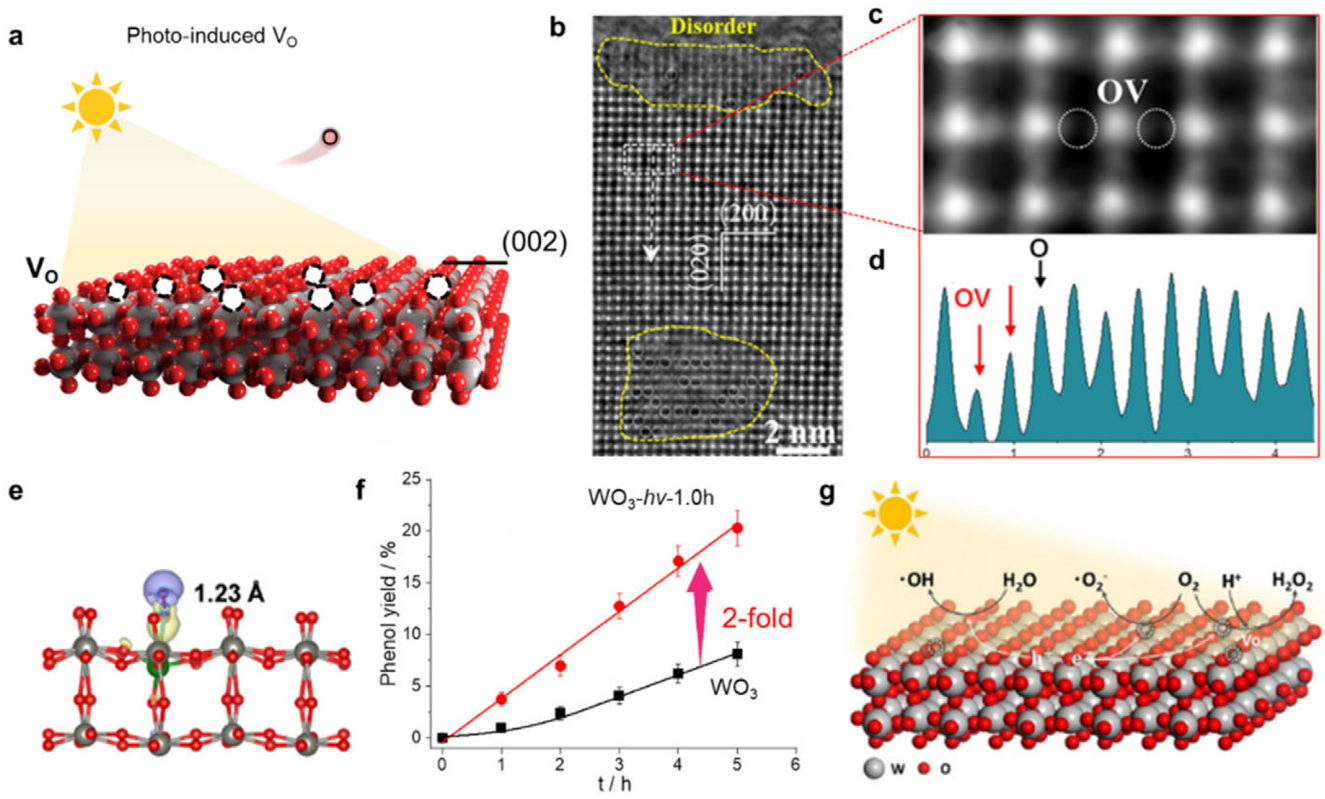


Figure 3. The atomic structure of (a) WO_3-$h\nu$-1.0 h samples, showing that the oxygen vacancies were produced on the (002) surface under illumination. (b) Integrated differential phase contrast (iDPC) image of the WO_3-$h\nu$-1.0 h sample along the [001] zone axis. (c) The enlarged iDPC image of the WO_3-$h\nu$-1.0 h sample at the surface area and (d) its corresponding intensity-line profiles. (e) DFT calculation of O_2 adsorbed on WO_3-$h\nu$-1.0 h sample. (f) The photocatalytic properties of the WO_3 and WO_3-$h\nu$-1.0 h samples over the benzene-to-phenol process under visible light. (g) Schematic illustration of O_2 and H_2O activation over WO_3-$h\nu$-1.0 h [84]. Reproduced with permission of Ref. [84] Copyright 2024, Wiley-VCH.

and facilitate charge transport [99,100]. Simultaneously, surface oxygen vacancies expose coordinatively unsaturated W sites and alter the local electronic structure, thereby enhancing the adsorption and activation of reactant molecules [42]. The accompanying local surface reconstruction can further create favorable adsorption configurations that stabilize reaction intermediates and reduce surface reaction barriers [19,101]. In contrast, excessive oxygen-vacancy concentrations may introduce deep traps or recombination centers, intensify carrier scattering, and trigger pronounced lattice distortion or structural reconstruction, ultimately suppressing charge separation and deteriorating structural stability [42]. Therefore, optimizing the concentration of oxygen vacancies, rather than simply maximizing their density, is critical for achieving a balanced enhancement of light harvesting, charge transport, surface reactivity, suppression of carrier recombination, and long-term structural stability [21].

V_O can also be engineered under high-pressure environments to regulate the distribution of V_O [60]. Since the γ-WO_3 sample was terminated with oxygen atoms, a great lattice compression was introduced on the sample under a pressure of 1.2 gigapascals (GPa) to facilitate the migration of surface oxygen atoms, constructing the abundant surface V_O on WO_{3-x} photocatalysts (Figure 4a–e) [60]. These surface-defined V_O on the WO_3 sample showed improved photocatalytic O_2 activation, further promoting the production of H_2O_2 (Figure 4f). It is concluded that precisely constructing surface V_O is a significant means to fortify the spatial charge separation and serves as an active site for the photocatalytic activation of O_2 under visible light. Recent studies further demonstrate a shift from the nonspecific generation of defects toward the spatial and chemical regulation of defect environments in WO_3-based photocatalysts. Pressure- and photo-mediated strategies have been employed to regulate the distribution of surface oxygen vacancies, while metal-vacancy engineering has been shown to modify the electronic structure and carrier transport behavior [56,81,89,97]. These advances highlight the importance of controlling not only defect concentration, but also defect location, local coordination environment, and electronic structure.

V_O can also play a vital role in tailoring the band structures of photocatalysts. Recently, Xie et al. reported that ultrathin cubic-WO_3 layers with rich oxygen structures (as boxed by a red dashed frame in Figure 5a,b) exhibited an intermediate band (IB) in the band gap, thereby lowering the band gap of the substrates and absorbing infrared light, which enables the infrared light-driven photocatalytic performances for CO_2 reduction reaction (Figure 5c, d) [43]. In addition to the anion vacancies, cation vacancies were generated through thermal evaporation and other methods in a reducing atmosphere. These defects play a crucial role in tuning the band structures by creating new electronic states near the valence band of the N-type semiconductor. This enhancement significantly improves the conductivity and bolsters carrier mobility within the photocatalyst. Liu et al. prepared WO_3 with W vacancies (V_W) through a chemical bath method, which can delocalize the valence band structures to reduce the effective mass of photogenerated holes for accelerating charge transport, thereby improving the

Downloaded from https://www.cambridge.org/core. 18 Nov 2026 at 09:38:25, subject to the Cambridge Core terms of use.

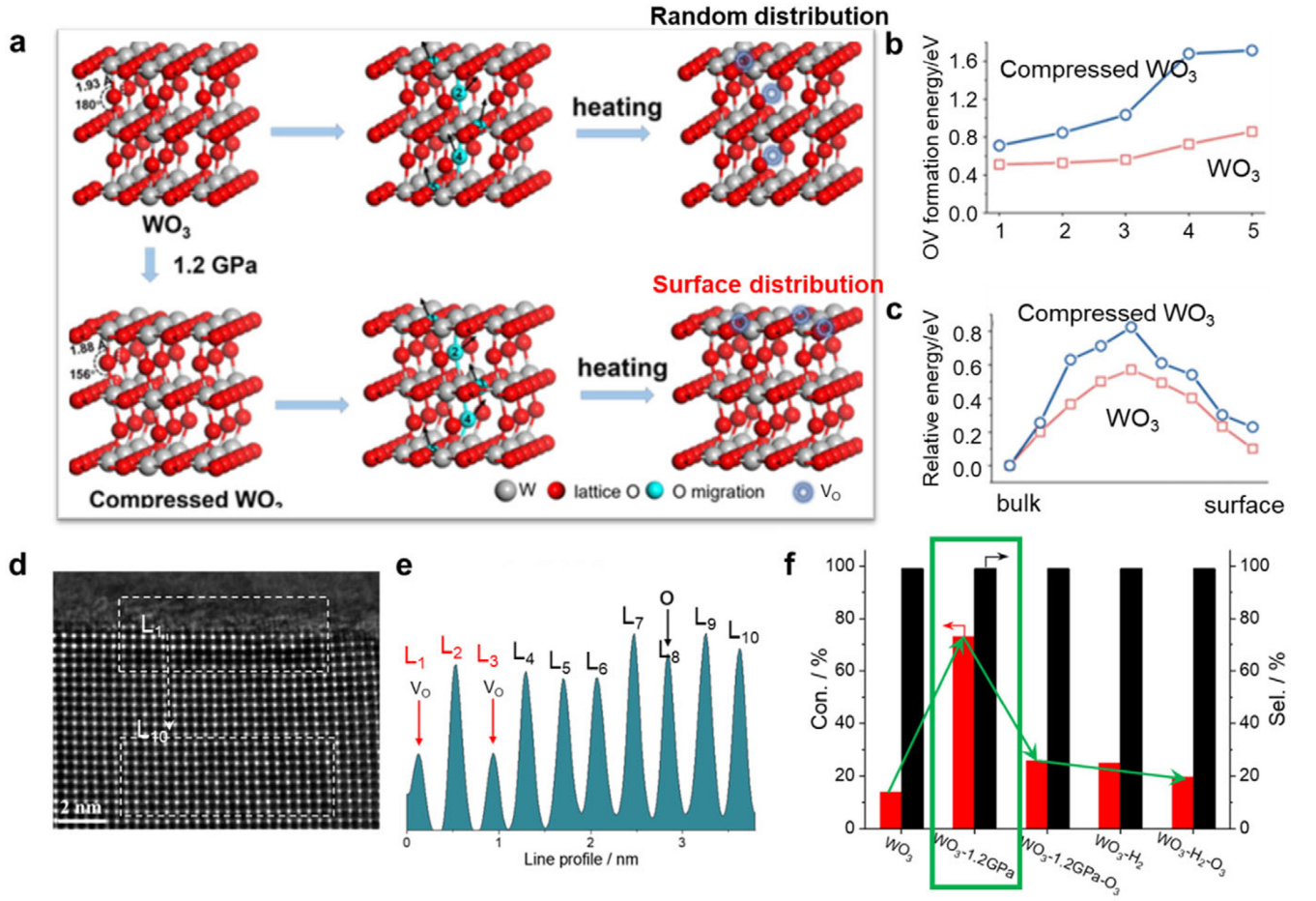


Figure 4. (a) Formation of V_O in WO_3 at ambient pressure (upper panel) and under 1.2 GPa (lower panel). (b) V_O formation energy of WO_3 as a function of oxygen layers. (c) Relative energy profiles of diffusion of the O from the bulk to the surface of WO_3. (d) The observed atomic structures of pressure-induced surface oxygen vacancies, and (e) their corresponding intensity-line profiles. (f) Photocatalytic H_2O_2 production rates of the WO_3 and V_O-rich WO_3 samples under visible irradiation [60]. Reproduced with permission of Ref. [60]. Copyright 2025, American Chemical Society.

photoelectrochemical water splitting performance (Figure 5e–h) [102]. In conclusion, constructing surface point defects with appropriate types, concentrations, and distributions on γ-WO_3 not only introduces defect levels in band structures to expand the absorption range of photocatalysts in visible light and enhance the dynamic transport of the photogenerated carrier, but also serves as a reaction site to capture photogenerated electrons for facilitating the activation of the molecules.

2.3. The Role of the Surface Line Defect

Surface line defects on photocatalysts are mainly derived from the surface steps and the surface terminations of planar defects (e. g., stacking faults) that existed in bulk [103]. They show lower-coordinated surface atoms to polarize the electronic structures of molecules as compared to the surface points [104,105]. These higher-concentration defects may produce continuous defect energy levels to broaden the light absorption range of the materials to the visible or even infrared region [43,106]. The surface line defects with one-dimensional geometry [107] can provide a continuous electron transport path to promote the directional migration of photogenerated carriers and restrict electron–hole recombination. Furthermore, the continuous structure of the surface line defect can disperse the reaction intermediates [108], reducing the risk of the active site being covered or deactivated on the isolated active site of the surface point defect [109,110].

As shown in Figure 6a–c, Xue et al. constructed the surface-ordered line defects identified as the terminations of the {013} stacking faults on the {002} surface of the WO_{3-x} photocatalysts (blue tungsten oxide) [19]. The integrated differential phase contrast (iDPC) image showed that the surface-ordered line defects expose plentiful quadri-coordinated W atoms, serving as the active sites for the adsorption and activation of CO_2 molecules, promoting the methanation desorption (Figure 6d). When the concentration of the surface-ordered line defect was increased by optimizing the heat treatment temperature, the photocatalytic properties of the monoclinic $WO_{2.9}$ sample were further improved.

To regulate the selectivity of CO products, Shen et al. reconstructed the surface-ordered line defect of the $WO_{2.9}$ sample to hexagonal-line defects (Figure 6e–g) [85]. The terminations of hexagonal-line defects on the {002} surfaces of the WO_{3-x} nanosheets varied the redox pathways of the *COOH intermediates, of which photogenerated carriers broke the C-O bonds, resulting in the main CH_4 product being changed to CO gas (Figure 6h). These results indicate that photocatalytic reaction pathways are strongly dependent on the atomic configurations and termination

Downloaded from https://www.cambridge.org/core. 18 Nov 2026 at 09:38:25, subject to the Cambridge Core terms of use.

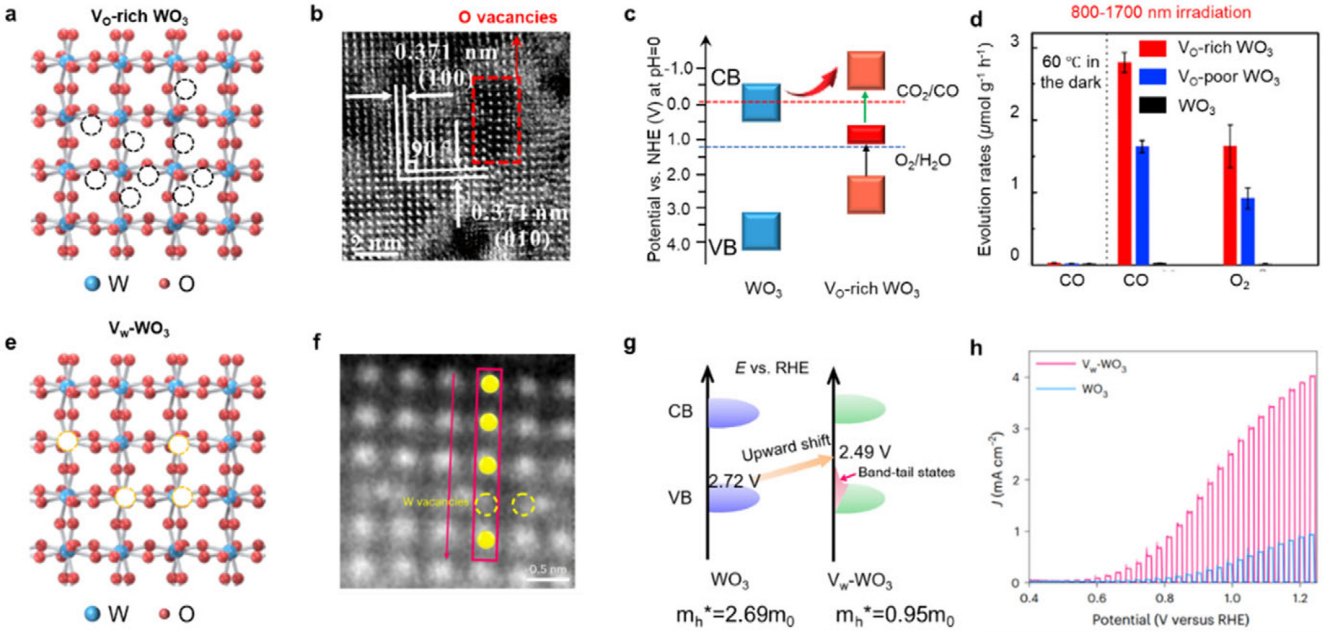


Figure 5. (a) Atomic model, (b) High-resolution TEM (HRTEM) image, (c) band structure illustration, and (d) photocatalytic properties of the ultra-thin WO_3 nanosheets with rich oxygen vacancies [43]. Reproduced with permission of Ref. [43]. Copyright 2018, Elsevier. (e) The atomic configuration, (f) Aberration-corrected high-angle annular dark field (AC-HAADF) image, and (g) band structure of the WO_3 sample with W vacancies. (h) The PEC water-splitting properties of the pristine WO_3 and V_W-WO_3 samples [102]. Reproduced with permission of Ref. [102]. Copyright 2025, Nature Publishing Group.

structures of surface defects. Recent studies published in 2024 further reveal that the local coordination environment generated by surface defect terminations is a key factor governing CO_2 photoreduction selectivity. Surface-ordered line defects terminating on the {002} facets of WO_{3-x} expose tetra-coordinated W sites, which promote cooperative CO_2 adsorption and favor deep hydrogenation toward CH_4 [19]. In contrast, reconstruction into hexagonal line defects produces distinct penta-coordinated W environments and modifies the conversion pathway of *COOH intermediates, thereby shifting the major product from CH_4 to CO [85]. These findings demonstrate that product selectivity is determined not simply by defect concentration, but also by the atomic configuration, termination structure, and local coordination environment of the defects.

2.4. The Role of Other Surface Defects

Generally, surface planar defects refer to the rough surface of photocatalysts, including nanoscale protrusions [111], nanopores [112], or nanopits [111]. In addition to greatly increasing the specific surface area to offer more reactive sites for reactant molecule activations or heteroatom loading, these microstructures also improve light energy utilization by extending the light path through multiple scattering effects [113]. Meanwhile, the surface planar defects can separate the redox reaction sites on the exposed facet to hinder the occurrence of back reactions [114] and decrease the diffusion length of the photogenerated carrier [115] for achieving spatial separation.

A representative example of the direct catalytic role of surface pits was reported by Liu et al., who constructed pothole-rich ultrathin WO_3 nanosheets for photocatalytic nitrate synthesis from N_2 [116]. The potholes disrupted the local surface periodicity and generated abundant dangling bonds and electronically active adsorption environments. These sites enhanced N_2 adsorption and polarization, thereby facilitating N ≡ N bond activation and subsequent nitrate formation. Under ambient conditions, the pothole-rich WO_3 nanosheets achieved an average nitrate-production rate of 1.92 mg g^{-1} h^{-1} without sacrificial agents or noble-metal cocatalysts (Figure 7a–d). This work demonstrates that surface potholes are not merely morphology-related features, but can generate distinct local coordination and electronic environments that directly participate in the activation of chemically inert molecules.

Zhang et al. reported Mo-doped $W_{18}O_{49}$ ultrathin nanowires with high-density V_O to promote the reduction of nitrogen under light irradiation (Figure 7e) [94]. These surface Mo adatoms integrated with adjacent W atoms exhibit asymmetric electronic structures, showing a large adsorption energy of nitrogen and converting to ammonia (Figure 7f–h). Zhang et al. have designed the Co-decorated $W_{18}O_{49}$ ultrathin nanowires to modify the energy configurations of substrates, making a significant upshift of the *d*-band center to produce more antibonding states above the Fermi level, thereby effectively adsorbing CO_2 molecules (Figure 7i–l) [93]. In fact, few investigations have exploited the roles of surface planar defects (rough surface) on photocatalytic reactions due to the limited strategies for precisely regulating the types and distribution of surface planar defects on photocatalysts. We believe that the development of chemical strategies to tailor the surface planar defect configuration has great applications in improving photocatalytic conversion efficiency.

Compared with point and line defects, the photocatalytic roles of extended surface irregularities remain less systematically understood because their atomic configurations and spatial distributions are difficult to regulate and characterize precisely. The pothole-rich WO_3 example demonstrates that local surface pits can generate chemically active coordination environments for molecular adsorption and bond activation. In parallel, heteroatom

Downloaded from https://www.cambridge.org/core. 18 Nov 2026 at 09:38:25, subject to the Cambridge Core terms of use.

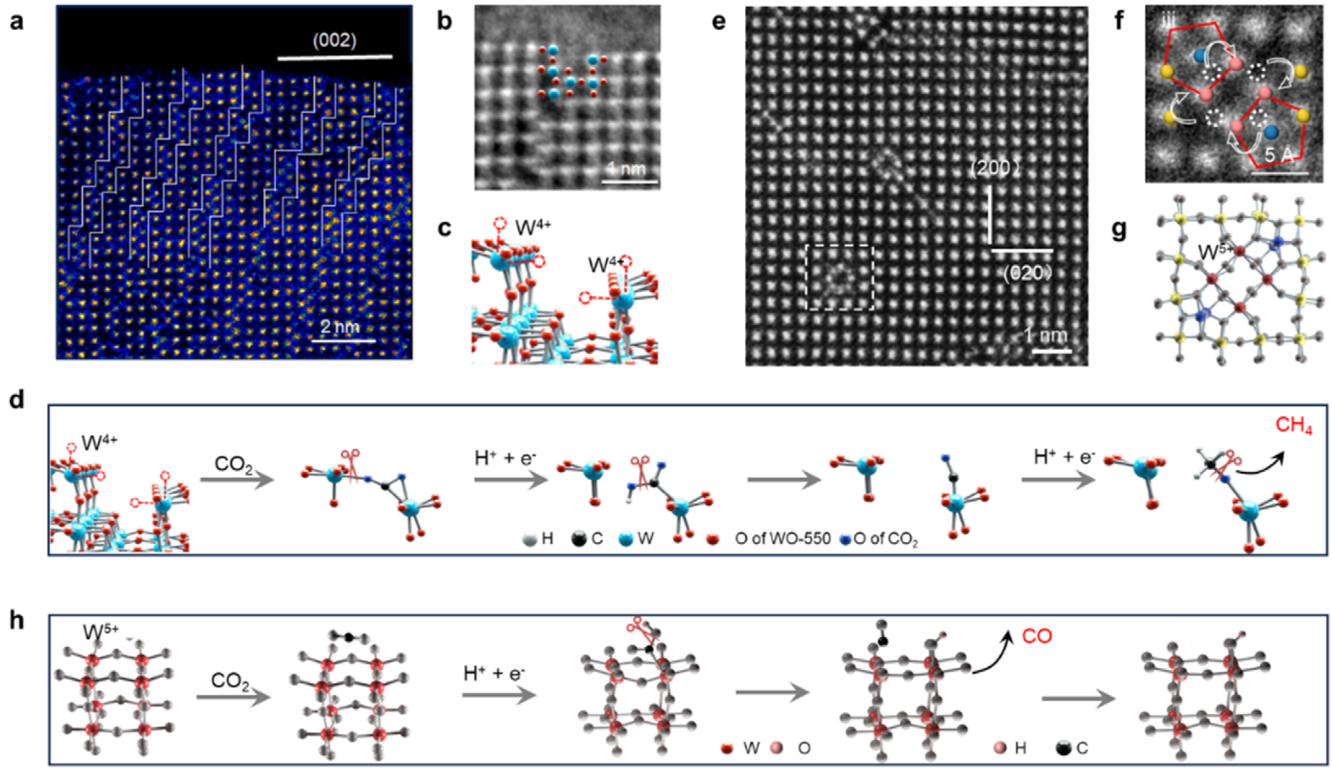


Figure 6. (a) AC-HAADF image, (b) enlarged iDPC image, (c) surface atomic structure of WO-550 sample at the termination of {002} surfaces, and (d) the reaction pathway of photoreduction of CO_2 molecules on the WO-550 sample with surface-ordered line defect for activating CO_2 molecules [19]. With permission of Ref. [19]. Copyright 2024, National Academy of Sciences. (e) AC-HAADF image, (f) enlarged iDPC image, and (g) atomic configuration of the WO_{3-x} nanosheets with hexagonal-line defects. (h) The reaction pathway of photoreduction of CO_2 molecules on the WO_{3-x} nanosheets with hexagonal-line defects [85]. With permission of Ref. [85] Copyright 2024, American Chemical Society.

incorporation provides a complementary strategy for modifying the local electronic structure and adsorption energetics of oxygen-deficient tungsten oxide surfaces. However, changes in neighboring W coordination environments depend on the dopant identity, defect configuration, and surface structure and should not be generalized as a universal effect. Future studies should distinguish the intrinsic contributions of surface roughness and potholes from those of isolated heteroatom sites using atomic-resolution and operando characterization.

The product selectivity of CO_2 photoreduction over defect-engineered WO_3-based photocatalysts is determined by the combined effects of defect configuration, surface termination, local W coordination, and intermediate adsorption geometry, rather than by defect dimensionality or concentration alone. Surface oxygen vacancies on selected WO_3 facets commonly expose penta-coordinated W sites, which facilitate *COOH formation and favor CO evolution. Ordered line defects derived from stacking-fault terminations expose tetra-coordinated W sites and enable cooperative W–O–C–W–O interactions, thereby enhancing CO_2 polarization and promoting deeper hydrogenation toward CH_4. Reconstruction into hexagonal line defects generates a distinct penta-coordinated W environment and modifies the conversion pathway of *COOH intermediates, redirecting product selectivity toward CO. In contrast, excessive structural reduction may induce reconstruction into stable, catalytically less active polyhedral configurations. These observations indicate that the atomic configuration and termination structure of surface defects are more reliable descriptors of product selectivity than defect dimensionality or concentration alone.

Defect engineering in WO_3 nanomaterials is crucial for enhancing photocatalytic performance by precisely tailoring their electronic structures, which in turn govern light absorption [41,117], charge separation [114,118], and reaction kinetics [43]. Unlike bulk defects, whose coordination environments are determined by the crystal lattice, bulk defects terminating at the surface generate unique coordination structures governed by the surface termination. These structure-specific environments dictate molecular adsorption and reactivity, making the termination of bulk defects critical for understanding photocatalytic reaction pathways in WO_3. It is therefore essential to clarify the role of unique surface geometric configurations—particularly those involving coordinated W atoms originating from low-dimensional defects—in governing reaction pathways, as summarized in Table 1 [9,19]. Typically, surface V_O on {002} facets exposes penta-coordinated W atoms, which activate molecular oxygen to form superoxide radicals [119]. In CO_2 photoreduction, such vacancies on flat surfaces promote CO production via the formation of single W–O bonds [43], while on high-index planes containing under-coordinated atoms, they induce CO_2 polarization through dual tilted W–O interactions. Line defects arising from stacking fault terminations on the {002} surface of $WO_{2.9}$ create tetra-coordinated W atoms at step edges, leading to the formation of W–O–C–W–O intermediates that bend the CO_2 configuration and favor CH_4 generation [19]. A shift to penta-coordinated W atoms within such defects redirects product selectivity toward CO [85]. Conversely, excessive

Downloaded from https://www.cambridge.org/core. 18 Nov 2026 at 09:38:25, subject to the Cambridge Core terms of use.

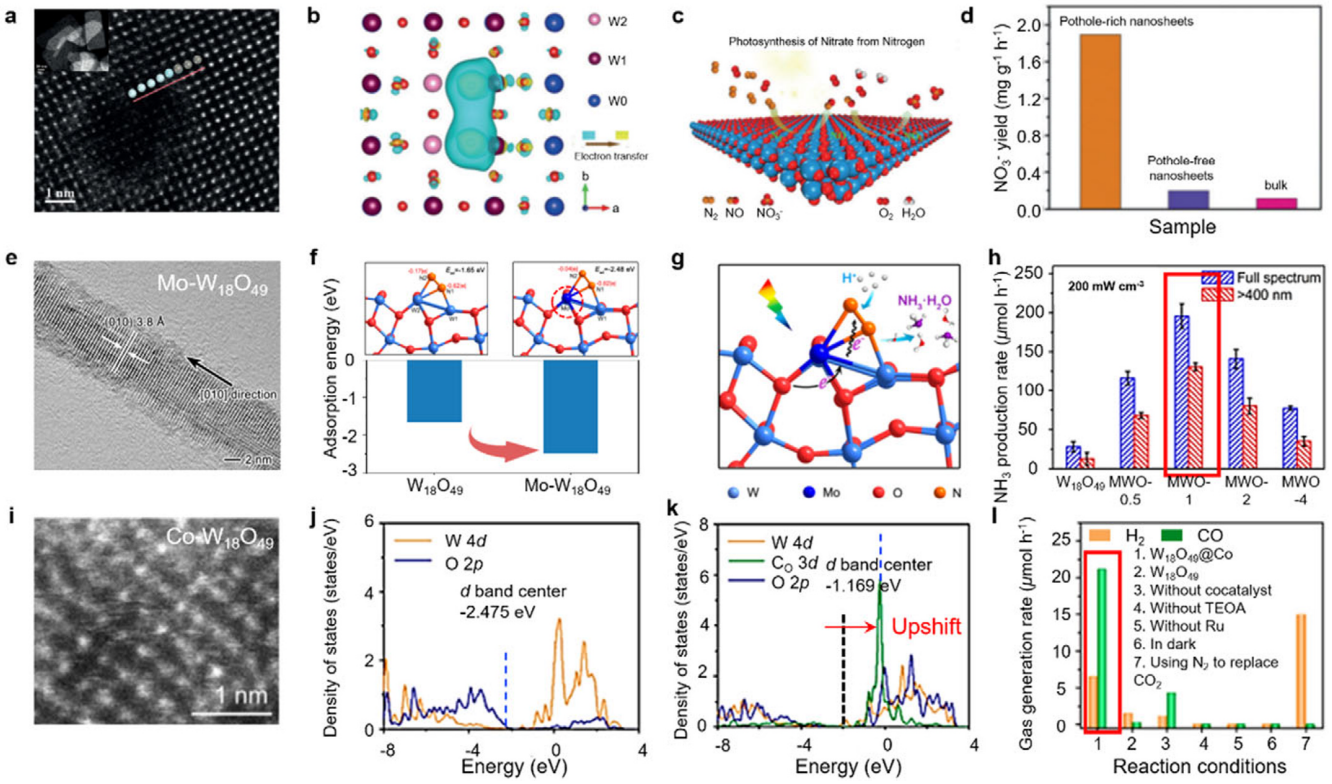


Figure 7. (a) Atomic-resolution HAADF-STEM image of a pothole-rich WO_3 nanosheet (inset is corresponding low-magnification HAADF image). (b) The charge difference density of the pothole-rich WO_3 nanosheet around the pothole region. (c) Schematic illustration of photoconversion of N_2 into nitrate at ambient conditions. (d) Nitrate formation rate calculated by the nitrate concentration profiles [116]. Reproduced with permission of Ref. [116]. Copyright 2019, Wiley-VCH. (e) HRTEM image of the Mo-doped $W_{18}O_{49}$ sample demonstrating rod-like morphology. (f) The adsorption configurations and energies of the surface-active sites of the $W_{18}O_{49}$ and Mo-doped $W_{18}O_{49}$ samples for capturing N_2 molecules. (g) Its reaction mechanism. (h) Photocatalytic ammonia production rates. Light irradiation conditions: full-spectrum or visible-NIR light ($\lambda > 400$ nm), 200 mW cm^{-2}, Na_2SO_3 as a sacrificial agent [94]. Reproduced with permission of Ref. [94]. Copyright 2018, American Chemical Society. (i) AC-HAADF image of Co-decorated $W_{18}O_{49}$ ultrathin nanowires. Calculated PDOS of (g) the pristine $W_{18}O_{49}$ and (k) Co-decorated $W_{18}O_{49}$ samples. (l) The photocatalytic CO_2 reduction performances of the Co-decorated $W_{18}O_{49}$ sample under various experimental conditions [93]. Reproduced with permission of Ref. [93]. Copyright 2021, American Chemical Society.

Table 1. Representative correlations among surface-defect configuration, local W coordination, CO_2 activation mode, key intermediates, and product selectivity in WO_3-based photocatalysts.

Proposed reaction pathways	C–O bond cleavage and CO desorption	CO_2 polarization and deep hydrogenation	Intermediate conversion suppresses methanation	$[WO_7]$ formation deactivates sites	Local electronic regulation of adsorption energetics
Major product	CO	CH_4	CO	Low activity	CO/H_2
Key intermediate	*COOH	Bent $*CO_2$/*CHO	*COOH		Depends on dopant
CO_2 activation mode	W–O	W–O–C–W–O	W^{5+}-O	Structural reconstruction	Enhanced chemisorption
W coordination	Penta-coordinated W	Tetra -coordinated W	Penta-coordinated W	Highly under-coordinated W	Tunable W coordination
Active site	W^{5+} adjacent to V_O	W^{4+} at the termination of ordered line defect	W^{5+} located at the hexagonal-tungsten line defect termination	Surface under-coordinated W	under-coordinated W neighboring heteroatom
Surfaces geometry	1D	2D	1D	2D	2D
Surface defect type	Oxygen vacancies	Ordered line defect	Hexagonal line defect	Excessively reduced surface	Heteroatom-decorated rough surface

Downloaded from https://www.cambridge.org/core. 18 Nov 2026 at 09:38:25, subject to the Cambridge Core terms of use.

reduction of the W coordination number (N ≤ 4) at stacking fault terminations on $WO_{2.72}$ surfaces induces structural reconstruction into stable [WO_7] decahedra, thereby deactivating the photocatalyst [19]. Hence, loading heteroatoms onto $WO_{2.72}$ surfaces represents an effective strategy for tuning the local coordination geometry of surface W atoms, enabling efficient photocatalytic conversion of target molecules [93,94].

Identifying the structures and active mechanisms of the surface defects at high spatial and temporal resolution can bridge the gap between atomic structures and catalytic properties. Over recent decades, numerous advances *in situ* spectroscopy techniques have been developed to probe the vibrational modes of chemical bonds between photocatalysts and adsorbates, facilitating the elucidation of photocatalytic CO_2 reduction mechanisms across diverse surface configurations at a macroscopic level.

Among these, *in situ* Fourier-transform infrared (FTIR) spectroscopy has been widely employed to identify key intermediates and infer reaction pathways. During the photoreduction of CO_2 coupled with water oxidation, the process typically involves carboxylation to form key *COOH intermediates, which subsequently interact with protons and photoexcited carriers to yield products such as CO, CH_4, and HCOOH. However, *in situ* FTIR spectroscopy offers limited accuracy in identifying the surface chemical states of photocatalysts. To address this, *quasi-in situ* or *in situ* X-ray photoelectron spectroscopy (XPS) has been utilized to monitor molecular adsorption behavior on photocatalyst surfaces under vacuum or controlled environments. These studies reveal that surface metal atoms exhibit high activity in capturing target molecules, and multiple surface atoms with dangling bonds can simultaneously interact with adsorbates via chemisorption on specific surface structures. Moreover, changes in the valence state of surface atoms have been detected when lattice atoms participate in photo-redox reactions. Because high-concentration defects can exert opposite effects on carrier dynamics depending on their type, concentration, and distribution, a combination of complementary characterization techniques is generally required to obtain a comprehensive understanding of charge-carrier behavior. Steady-state photoluminescence (PL) and time-resolved photoluminescence (TRPL) are commonly employed to evaluate radiative recombination and carrier lifetimes. Transient photocurrent response and electrochemical impedance spectroscopy (EIS) provide insights into charge separation efficiency and interfacial charge-transfer kinetics (Table 2). Surface photovoltage (SPV) spectroscopy enables direct visualization of photoinduced charge separation and migration near semiconductor surfaces, whereas femtosecond and nanosecond transient absorption (TA) spectroscopy captures ultrafast carrier trapping, transfer, and recombination processes over broad temporal scales (Table 2). The combined application of these techniques allows the intrinsic relationship between defect structures and carrier dynamics to be established more reliably than any individual characterization method alone. Given that the migration of photoexcited carriers occurs on picosecond to nanosecond timescales, ultrafast transient absorption spectroscopy has been employed to trace the transport of carriers from the bulk to the surface. To further probe proton-coupled electron transfer during reactions, *in situ* Raman spectroscopy has proven effective in identifying the chemical states of electrons and lattice phonons. Preliminary experimental results indicate that protons are injected into the gaps of corner-sharing [WO_6] octahedra when photoexcited electrons migrate to the surface—challenging the conventional view that protons react solely with target molecules on the surface.

Table 2. Complementary characterization techniques for resolving defect structures, surface chemical states, and charge-carrier dynamics in defect-engineered WO_3 photocatalysts.

Characterization technique	Primary information	Quantitative capability	Spatial level	Temporal scale	Main limitation
iDPC-STEM	Atomic arrangement, defect termination, local coordination	Mostly qualitative	Single particle/ atomic level	Qualitative	Single particle
XPS	Chemical state (W^{5+}/W^{6+}, O vacancy)	Semi-quantitative	Surface averaged	Semi-quantitative	Surface averaged
EPR	Unpaired electrons/oxygen vacancies	Semi-quantitative	Bulk averaged	Semi-quantitative	Bulk averaged
Raman/PL spectroscopy	Lattice distortion, defect states, radiative recombination	Qualitative to semi-quantitative	Bulk/Local	Qualitative	Bulk/Local
CL/KPFM mapping	Local electronic activity, work-function or potential variation	Indirect	Nanoscale mapping	Indirect	Nanoscale mapping
TRPL	Carrier lifetime and recombination kinetics	Model-dependent	Bulk averaged	ps–ns	Lifetime does not uniquely identify transport pathway
Transient photocurrent	Photoinduced charge extraction/ separation response	Comparative	Device/electrode averaged	ms–s	Strongly affected by electrode architecture
EIS	Interfacial charge-transfer resistance and capacitance	Equivalent-circuit dependent	Device/electrode averaged	Frequency domain	Model ambiguity
SPV	Surface charge separation and migration direction	Comparative	Surface averaged/ mapped	μs–s, method dependent	Interpretation depends on surface states
Transient absorption	Carrier trapping, transfer, and recombination	Kinetic modeling	Ensemble averaged	fs–ms	Spectral assignment can be complex

Downloaded from https://www.cambridge.org/core. 18 Nov 2026 at 09:38:25, subject to the Cambridge Core terms of use.

Table 3. Summary of representative defect-engineered WO_3-based photocatalysts, including defect construction, structural characteristics, electronic regulation, photocatalytic performance, and stability.

Stability issue	10 cycles	12 cycles	9 cycles	Stable over 120 h	6 cycles	9 cycles
Performance enhancement	~2-fold enhancement	~2.3-fold enhancement	Enables IR-light-driven CO_2 reduction	Higher photocurrent than pristine WO_3	inactive $WO_3 \rightarrow$ 8.2 μmol CH_4	Product selectivity switched from CH_4 to CO
Major product	Phenol	H_2O_2	CO	O_2	CH_4	CO
Target reaction	Benzene oxidation	O_2 reduction	CO_2 reduction	Water oxidation	CO_2 reduction	CO_2 reduction
Band-structure/carrier modulation	Defect states; charge separation	charge separation	Intermediate band; IR absorption	Valence-band delocalization	CB upshift; charge transport	Modified *COOH pathway
Primary active site	Unsaturated W	Exposed W	Vacancy-related W	W-vacancy sites	Tetra-coordinated W	Penta-coordinated W
Main characterization methods	iDPC-STEM, XPS/EPR, DFT	STEM, DFT	HRTEM, UV–vis, DFT	AC-HAADF, DFT	AC-HAADF, iDPC, DFT	AC-HAADF, iDPC, DFT
Preparation/defect-construction method	Photo-reduction	High-pressure treatment	Defective ultrathin WO_3 synthesis	Chemical-bath synthesis	H_2/Ar reduction	S atmosphere reduction
Defect type and location	Surface V_O	Surface V_O	V_O-related states	W vacancies	Line defects on {002}	Hexagonal line defects
Representative material	Photoinduced V_O-rich WO_3	Pressure-induced WO_3	Ultrathin cubic WO_3	W-vacancy WO_3	$WO_{2.9}$ with ordered line defects	WO_{3-x} with hexagonal line defects

Stability issue	Stable over 30 h	5 cycles	4 cycles	Stable over 10 h
Performance enhancement	≈9.8-fold higher than pothole-free WO_3	3-fold higher NH_3 yield than $W_{18}O_{49}$	~10-fold higher than $W_{18}O_{49}$	≈3–fold higher phenol yield than WO_3
Major product	NO_3^-	NH_3	CO and H_2	Phenol
Target reaction	Nitrate photosynthesis	N_2 fixation	CO_2 reduction	Benzene oxidation
Band-structure/carrier modulation	Local charge redistribution	Refined defect states	d-band shift	Enhanced O_2 activation
Primary active site	Pothole dangling bonds	Mo–W–O sites	Co sites	Mo-V_O sites
Main characterization methods	HAADF, DFT	HRTEM, DFT	AC-HAADF, XPS/XAS, DFT	STEM, XPS/EPR, DFT
Preparation/defect-construction method	Thermal treatment	solvothermal method	A solvothermal coupled with chemical-bath method	Thermal treatment coupled with irradiation
Defect type and location	Surface potholes	Mo-modified defects	Isolated Co sites	Mo + surface V_O
Representative material	Pothole-rich ultrathin WO_3	Mo-doped $W_{18}O_{49}$ nanowires	Co-decorated $W_{18}O_{49}$ nanowires	Mo-incorporated WO_3 with photoinduced V_O

Note: The reported performance values were obtained under different reaction conditions and should not be directly compared across different photocatalytic systems. "Not systematically evaluated" indicates that long-term defect stability or operando structural evolution was not explicitly examined in the corresponding study. Reference numbers should be updated after the final reference list is reordered.

Collectively, findings from electron microscopy at the microscopic level and *in situ* spectroscopy at the macroscopic scale establish that the spatial freedom of surface W atoms, governed by coordination number and surface atomic geometry, serves as a key regulator for overcoming rate-determining steps in photocatalytic reactions. This mechanistic insight underscores the need for a comprehensive database correlating defect geometries with reaction pathways, which will facilitate the rational design of defect-engineered photocatalysts and reduce reliance on empirical optimization. To provide a more systematic comparison, representative defect-engineered WO_3-based photocatalysts are summarized in Table 3, including defect type, preparation method, characterization technique, primary active site, electronic/carrier modulation, target reaction, major product, performance enhancement, and photocatalytic stability.

2.5. Summary and Outlook

In this mini-review, we have explored the structures and evolutionary mechanisms of surface defects in WO_3 photocatalysts. The impact of these defects on the photocatalytic reaction process was also investigated, including light-absorption properties, dynamic charge-transport behavior, surface adsorption, and reaction processes. Furthermore, we summarize various types of dimensional surface defects, providing insights into their atomic-level mechanisms in photocatalytic environments. This mini-review aims to

Downloaded from https://www.cambridge.org/core. 18 Nov 2026 at 09:38:25, subject to the Cambridge Core terms of use.

offer a comprehensive outlook on defect engineering, addressing four key aspects.

1. Atomic-level regulation of defect structures. To date, the fabrication of surface defects primarily relies on methods such as high-temperature treatment, liquid-phase reduction, ion exchange, plasma etching, and photochemical processes. However, achieving precise control over the type, concentration, and distribution of surface defects remains a significant challenge. Future research may leverage machine learning and high-throughput computational techniques, coupled with advanced atomic-resolution characterization methods (e.g., aberration-corrected transmission electron microscopy and X-ray absorption fine structure spectroscopy), to optimize defect engineering strategies and enable the controlled design of defects in photocatalysts. A major challenge is that the formation of a target defect is often accompanied by defect migration, aggregation, lattice relaxation, surface reconstruction, or the generation of coupled defects. Therefore, independently controlling defect type, concentration, spatial location, and termination structure remains difficult. Future synthesis strategies should move beyond empirical reduction treatments toward quantitatively controlled and site-selective defect engineering.
2. The interactive influence of defect types, concentrations, and distributions. Surface defects disrupt the periodic atomic structures of photocatalysts, leading to the formation of defect energy levels that can facilitate the dynamic behavior of photogenerated charge carriers. However, defects at high concentrations, or bulk defects, may act as recombination centers, thereby hindering charge separation. Thus, it is essential to investigate the relationship between the type, concentration, and distribution of surface defects and the dynamic behavior of photogenerated carriers under operational conditions. Quantitative identification of these defect parameters also remains challenging because most characterization techniques provide either localized atomic-scale information or ensemble-averaged signals. It is therefore difficult to simultaneously determine defect concentration, spatial distribution, local coordination environment, and dynamic evolution under reaction conditions. Combining atomic-resolution imaging with quantitative spectroscopy and operando measurements will be essential for establishing reliable correlations between defect structures and charge-carrier behavior. Such studies are crucial for guiding the rational design of defective photocatalysts.
3. The stability of the surface defects. While defects can enhance photocatalytic activity, certain defects—such as high-concentration oxygen vacancies—may undergo reconstruction or disappear over extended operational periods, leading to a decrease in catalytic activity. Future research should prioritize the investigation of defect stability under realistic operating conditions, employing advanced *in situ* characterization techniques and theoretical modeling. This approach will provide insights into self-repair mechanisms and dynamic regulation strategies for defects, enabling precise control over defect evolution during photocatalytic cycles. Such advancements will improve the operational longevity and reliability of photocatalysts, thus facilitating their use in sustainable energy and environmental applications. The design of the photocatalyst in the future should go beyond isolated investigations of individual defect types to fully elucidate the synergistic interactions among multiscale defects (e.g., cooperative effects between surface point vacancies and atomic-level step edges). Moreover, integrating these insights with complementary modification strategies, such as heterojunction formation, interfacial engineering, and surface functionalization, will be crucial for advancing photocatalyst performance.
4. Data-driven and operando understanding of dynamic defects. Future research should establish dynamic defect databases that correlate defect configurations, spatial distributions, evolution pathways, and catalytic performance under operating conditions. Integrating these databases with artificial intelligence and high-throughput calculations may enable the prediction, screening, and controllable synthesis of target defect structures. Meanwhile, advanced operando characterization techniques are required to directly monitor the formation, reconstruction, migration, and deactivation of active defects under realistic reaction conditions. Such efforts will facilitate the establishment of quantitative defect–structure–activity relationships and accelerate the rational design of defect-engineered WO_3-based photocatalysts.

Open peer review. To view the open peer review materials for this article, please visit http://doi.org/10.1017/S2978169826000008.

Author contributions. M.S., S.X., Z.Y., and C.Y. wrote the first draft of the manuscript. Z.Y., and C.Y. were in charge of the manuscript. All authors contributed to the discussion and writing of this minireview.

Acknowledgments. C. Y., Z. Y., and S. X. acknowledge support from the National Natural Science Foundation of China (22272027, 52201006, 22272024, 22402033). This work was also supported by the Science Fund for Creative Research Groups of the National Natural Science Foundation of China (Grant No. 22621101).

Competing interests. The authors declare that they have no competing interests.

Data availability statement. The data that support the findings of this study are available from the corresponding author upon reasonable request.

References

1. H. Rao, L. C. Schmidt, J. Bonin and M. Robert, 'Visible-light-driven methane formation from CO_2 with a molecular iron catalyst'. *Nature*, 548: (2017), 74–77.
2. S. N. Habisreutinger, L. Schmidt-Mende and J. K. Stolarczyk, 'Photocatalytic reduction of CO_2 on TiO_2 and other semiconductors'. *Angewandte Chemie International Edition*, 52: (2013), 7372–7408.
3. S. Xue, H. Tang, M. Shen et al., 'Establishing multiple-order built-in electric fields within heterojunctions to achieve photocarrier spatial separation'. *Advanced Materials*, 36: (2024), 2311937.
4. J. Yang, D. Wang, H. Han and C. Li, 'Roles of cocatalysts in photocatalysis and photoelectrocatalysis'. *Accounts of Chemical Research*, 46: (2013), 1900–1909.
5. J. Ran, J. Zhang, J. Yu, M. Jaroniec and S. Z. Qiao, 'Earth-abundant cocatalysts for semiconductor-based photocatalytic water splitting'. *Chemical Society Reviews*, 43: (2014), 7787–7812.
6. B. Dong, J. Cui, Y. Qi and F. Zhang, 'Nanostructure engineering and modulation of (oxy) nitrides for application in visible-light-driven water splitting'. *Advanced Materials*, 33: (2021), 2004697.
7. S. Bai, N. Zhang, C. Gao and Y. Xiong, 'Defect engineering in photocatalytic materials'. *Nano Energy*, 53: (2018), 296–336.
8. J. Xiong, J. Di, J. Xia, W. Zhu and H. Li, 'Surface defect engineering in 2D nanomaterials for photocatalysis'. *Advanced Functional Materials*, 28: (2018), 1801983.
9. Z. Zafar, S. Yi, J. Li et al., 'Recent development in defects engineered photocatalysts: an overview of the experimental and theoretical strategies'. *Energy and Environmental Materials*, 5: (2022), 68–114.
10. H. Zhuzhang, X. Liang, J. Li et al., 'Precise manipulation on the structural defects of Poly (Triazine Imide) single crystals for efficient photocatalytic

Downloaded from https://www.cambridge.org/core. 18 Nov 2026 at 09:38:25, subject to the Cambridge Core terms of use.

overall water splitting'. *Angewandte Chemie International Edition*, 64: (2025), e202421861.
11. E. Pastor, M. Sachs, S. Selim et al., 'Electronic defects in metal oxide photocatalysts'. *Nature Reviews Materials*, 7: (2022), 503–521.
12. J. H. Park and J.-H. Kim, 'Selective CO_2 photoconversion on low-coordinate TiO_2'. *Chem*, 6: (2020), 2435–2436.
13. X. Li, Y. Sun, J. Xu et al., 'Selective visible-light-driven photocatalytic CO_2 reduction to CH_4 mediated by atomically thin $CuIn_5S_8$ layers'. *Nature Energy*, 4: (2019), 690–699.
14. Y. Zhang, B. Xia, J. Ran, K. Davey and S. Z. Qiao, 'Atomic-level reactive sites for semiconductor-based photocatalytic CO_2 reduction'. *Advanced Functional Materials*, 10: (2020), 1903879.
15. Y. He, Q. Lei, C. Li et al., 'Defect engineering of photocatalysts for solar-driven conversion of CO_2 into valuable fuels'. *Materials Today*, 50: (2021), 358–384.
16. Q. Liu, F. Wang, H. Lin et al., 'Tungsten trioxide as an electrode for photoelectrolysis of water'. *Solid State Communications*, 19: (1976), 1011–1014.
17. W. Guo, Q. Wei, G. Li, F. Wei and Z. Hu, 'A bulk oxygen vacancy dominating WO_{3-x} photocatalyst for carbamazepine degradation'. *Nanomaterials*, 14: (2024), 923.
18. H. Kong, H. Yang, J. S. Park et al., 'Spatial control of oxygen vacancy concentration in monoclinic WO_3 photoanodes for enhanced solar water splitting'. *Advanced Functional Materials*, 32: (2022), 2204106.
19. S. Xue, C. Wei, M. Shen et al., 'Enriching surface-ordered defects on WO_3 for photocatalytic CO_2-to-CH_4 conversion by water'. *Proceedings National Academy of Sciences of the United States of America*, 121: (2024), e2319751121.
20. P. Zhu, X. Sun, Y. Wang et al., 'Multifunctional oxygen vacancies in WO_{3-x} for catalytic alkylation of C–H by alcohols under red-light'. *Journal of Catalysis*, 402: (2021), 208–217.
21. S. Corby, L. Francàs, A. Kafizas and J. R. Durrant, 'Determining the role of oxygen vacancies in the photoelectrocatalytic performance of WO_3 for water oxidation'. *Chemical Science*, 11: (2020), 2907–2914.
22. W. Wang, A. Janotti and C. G. Van de Walle, 'Role of oxygen vacancies in crystalline WO_3'. *Journal of Materials Chemistry C*, 4: (2016), 6641–6648.
23. J. Zhu, M. Vasilopoulou, D. Davazoglou et al., 'Intrinsic defects and H doping in WO_3'. *Scientific Reports*, 7: (2017), 40882.
24. X. Ye, C. Wei, S. Xue et al., 'Atomistic observation of temperature-dependent defect evolution within sub-stoichiometric WO_{3-x} catalysts'. *ACS Applied Materials & Interfaces*, 14: (2021), 2194–2201.
25. M. Butler, R. Nasby and R. K. Quinn, 'Tungsten trioxide as an electrode for photoelectrolysis of water'. *Solid State Communications*, 19: (1976), 1011–1014.
26. H. Reiche, W. W. Dunn and A. J. Bard, 'Heterogeneous photocatalytic and photosynthetic deposition of copper on titanium dioxide and tungsten (VI) oxide powders'. *The Journal of Physical Chemistry*, 83: (1979), 2248–2251.
27. K. Villa, S. Murcia-López, T. Andreu and J. R. Morante, 'Mesoporous WO_3 photocatalyst for the partial oxidation of methane to methanol using electron scavengers'. *Applied Catalysis B: Environment and Energy*, 163: (2015), 150–155.
28. H. Wang, L. Zhang, K. Wang, X. Sun and W. Wang, 'Enhanced photocatalytic CO_2 reduction to methane over $WO_3{\cdot}0.33\ H_2O$ via Mo doping'. *Applied Catalysis B: Environment and Energy*, 243: (2019), 771–779.
29. B. Aurian-Blajeni, M. Halmann and J. Manassen, 'Photoreduction of carbon dioxide and water into formaldehyde and methanol on semiconductor materials'. *Solar Energy*, 25: (1980), 165–170.
30. J. Kim, C. W. Lee and W. Choi, 'P platinized WO_3 as an environmental photocatalyst that generates OH radicals under visible light, *environ*'. *Science and Technology*, 44: (2010), 6849–6854.
31. Y. Fan, Y. Jiang, H. Lin et al., 'Insight into selectivity of photocatalytic methane oxidation to formaldehyde on tungsten trioxide'. *Nature Communications*, 15: (2024), 4679.
32. T. H. Jeon, D. Monllor–Satoca, G. Moon et al., 'Ag(I) ions working as a hole-transfer mediator in photoelectrocatalytic water oxidation on WO_3 film'. *Nature Communications*, 11: (2020), 967.
33. A. M. Mohamed, S. A. Shaban, H. A. E. Sayed, B. E. Alanadouli and N. K. Allam, 'Morphology-photoactivity relationship: WO_3 nanostructured films for solar hydrogen production'. *International Journal of Hydrogen Energy*, 41: (2016), 866–872.
34. I. Bedja, S. Hotchandani and P. V. Kamat, 'Photoelectrochemistry of quantized WO_3 colloids: electron storage, electrochromic, and photoelectrochromic effects'. *The Journal of Physical Chemistry*, 97: (2002), 11064–11070.
35. M. Wang, G. Tan, S. Feng et al., 'Defects and internal electric fields synergistically optimized g-C_3N_{4-x}/BiOCl/$WO_{2.92}$ heterojunction for photocatalytic NO deep oxidation'. *Journal of Hazardous Materials*, 408: (2021), 124897.
36. X. Zhao, X. Zhang, D. Han and L. Niu, 'Ag-supported Z-scheme $WO_{2.9}$/g-C_3N_4 composite photocatalyst for photocatalytic degradation under visible light'. *Applied Surface Science*, 501: (2020), 144258.
37. Z. Xue, X. Jia, X. Gao et al., 'Regulating the electronic status on open $WO_{2.83}$ surfaces for ultrasensitive H_2S sensors'. *Sensors & Actuators, B: Chemical*, 385: (2023), 133569.
38. X. Guo, X. Qin, Z. Xue et al., 'Morphology-controlled synthesis of $WO_{2.72}$ nanostructures and their photocatalytic properties'. *RSC Advances*, 6: (2016), 48537–48542.
39. B. Li, X. Shao, T. Liu, L. Shao and B. Zhang, 'Construction of metal/$WO_{2.72}$/rGO ternary nanocomposites with optimized adsorption, photocatalytic, and photoelectrochemical properties'. *Applied Catalysis B: Environment and Energy*, 198: (2016), 325–333.
40. Z. Chen, Q. Wang, H. Wang et al., 'Ultrathin PEGylated $W_{18}O_{49}$ nanowires as a new 980 nm-laser-driven photothermal agent for efficient ablation of cancer cells in vivo'. *Advanced Materials*, 25: (2013), 2095–2100.
41. J. Yan, T. Wang, G. Wu et al., 'Tungsten oxide single crystal nanosheets for enhanced multichannel solar light harvesting'. *Advanced Materials*, 27: (2015), 1580–1586.
42. K. Kato, Y. Uemura, K. Asakura and A. Yamakata, 'Role of oxygen vacancy in the photocarrier dynamics of WO_3 photocatalysts: the case of recombination centers'. *Journal of Physical Chemistry C*, 126: (2022), 9257–9263.
43. L. Liang, X. Li, Y. Sun et al., 'Infrared light-driven CO_2 overall splitting at room temperature'. *Joule*, 2: (2018), 1004–1016.
44. H. Zheng, J. Z. Ou, M. S. Strano et al., 'Nanostructured tungsten oxide-properties, synthesis, and applications'. *Advanced Functional Materials*, 21: (2011), 2175–2196.
45. K. S. Joya, Y. F. Joya, K. Ocakoglu and R. van de Krol, 'Water-splitting catalysis and solar fuel devices: artificial leaves on the move'. *Angewandte Chemie International Edition*, 52: (2013), 10426–10437.
46. P. Shandilya, S. Sambyal, R. Sharma, P. Mandyal and B. Fang, 'Properties, optimized morphologies, and advanced strategies for photocatalytic applications of WO_3 based photocatalysts'. *Journal of Hazardous Materials*, 428: (2022), 128218.
47. Y. Bu, J. Ren, H. Zhang et al., 'Photogenerated-carrier separation along edge dislocation of WO_3 single-crystal nanoflower photoanode'. *Journal of Materials Chemistry A*, 6: (2018), 8604–8611.
48. S. Zhang, Y. Si, B. Li et al., 'Atomic-level and modulated interfaces of photocatalyst heterostructure constructed by external defect-induced strategy: a critical review'. *Small*, 17: (2021), 2004980.
49. Y. Xue, P. Shao, M. Lin et al., 'Tailoring S-vacancy concentration changes the type of the defect and photocatalytic activity in ZFS'. *Journal of Hazardous Materials*, 428: (2022), 128215.
50. N. Zhang, C. Gao and Y. Xiong, 'Defect engineering: defect engineering: a versatile tool for tuning the activation of key molecules in photocatalytic reactions'. *Journal of Energy Chemistry*, 37: (2019), 43–57.
51. A. Al Mohammad and M. Gillet, 'Phase transformations in WO_3 thin films during annealing'. *Thin Solid Films*, 408: (2002), 302–309.
52. C. Ramana, S. Utsunomiya, R. Ewing, C. Julien and U. Becker, 'Structural stability and phase transitions in WO_3 thin films'. *The Journal of Physical Chemistry B*, 110: (2006), 10430–10435.
53. C. Di Valentin and G. Pacchioni, 'Spectroscopic properties of doped and defective semiconducting oxides from hybrid density functional calculations'. *Accounts of Chemical Research*, 47: (2014), 3233–3241.

Downloaded from https://www.cambridge.org/core. 18 Nov 2026 at 09:38:25, subject to the Cambridge Core terms of use.

54. E. K. Salje, S. Rehmann, F. Pobell et al., 'Crystal structure and paramagnetic behaviour of ε-WO_{3-x}'. *Journal of Physics: Condensed Matter*, 9: (1997), 6563.
55. T. Vogt, P. M. Woodward and B. A. Hunter, 'The high-temperature phases of WO_3'. *Journal of Solid State Chemistry*, 144: (1999), 209–215.
56. C. Granqvist, 'Electrochromic materials: microstructure, electronic bands, and optical properties'. *Applied Physics a: Materials Science & Processing*, 57: (1993), 3–12.
57. W. Li, P. Da, Y. Zhang et al., 'WO_3 nanoflakes for enhanced photoelectrochemical conversion'. *ACS Nano*, 8: (2014), 11770–11777.
58. Q. Mi, A. Zhanaidarova, B. S. Brunschwig, H. B. Gray and N. S. Lewis, 'A quantitative assessment of the competition between water and anion oxidation at WO_3 photoanodes in acidic aqueous electrolytes'. *Energy & Environmental Science*, 5: (2012), 5694–5700.
59. D. Li, R. Chen, S. Wang et al., 'Unraveling the kinetics of photocatalytic water oxidation on WO_3'. *Journal of Physical Chemistry Letters*, 11: (2019), 412–418.
60. X. Wang, S. Xue, M. Huang et al., 'Pressure-induced engineering of surface oxygen vacancies on metal oxides for heterogeneous photocatalysis'. *Journal of the American Chemical Society*, 147: (2025), 4945–4951.
61. A. Yella, M. N. Tahir, S. Meuer et al., 'Synthesis, characterization, and hierarchical organization of tungsten oxide nanorods: spreading driven by Marangoni flow'. *Journal of the American Chemical Society*, 131: (2009), 17566–17575.
62. G. Wang, Y. Ling, H. Wang et al., 'Hydrogen-treated WO_3 nanoflakes show enhanced photostability'. *Energy & Environmental Science*, 5: (2012), 6180–6187.
63. C. Santato, M. Odziemkowski, M. Ulmann and J. Augustynski, 'Crystallographically oriented mesoporous WO_3 films: synthesis, characterization, and applications'. *Journal of the American Chemical Society*, 123: (2001), 10639–10649.
64. J. Polleux, N. Pinna, M. Antonietti and M. Niederberger, 'Growth and assembly of crystalline tungsten oxide nanostructures assisted by bioligation'. *Journal of the American Chemical Society*, 127: (2005), 15595–15601.
65. D. Chandra, K. Saito, T. Yui and M. Yagi, 'Crystallization of tungsten trioxide having small mesopores: highly efficient photoanode for visible-light-driven water oxidation'. *Angewandte Chemie International Edition*, 52: (2013), 12606–12609.
66. A. Polaczek, M. Pekala and Z. Obuszko, 'Magnetic susceptibility and thermoelectric power of tungsten intermediary oxides'. *Journal of Physics: Condensed Matter*, 6: (1994), 7909.
67. V. Makarov and M. Trontelj, 'Sintering and electrical conductivity of doped WO_3'. *Journal of the European Ceramic Society*, 16: (1996), 791–794.
68. S. Bandi and A. K. Srivastav, 'Oxygen-deficient tungsten oxides'. *Journal of Materials Science*, 56: (2021), 6615–6644.
69. D. Migas, V. Shaposhnikov, V. Borisenko and T. oxides, 'The metallic nature of Magnéli phases'. *Journal of Applied Physics*, 108: (2010), 093714.
70. G. A. Niklasson, L. Berggren and A.-L. Larsson, 'Electrochromic tungsten oxide: the role of defects'. *Solar Energy Materials & Solar Cells*, 84: (2004), 315–328.
71. K. Manthiram and A. P. Alivisatos, 'Tunable localized surface plasmon resonances in tungsten oxide nanocrystals'. *Journal of the American Chemical Society*, 134: (2012), 3995–3998.
72. Y. Lu, Y. Jiang, X. Gao, X. Wang and W. Chen, 'Strongly coupled pd nanotetrahedron/tungsten oxide nanosheet hybrids with enhanced catalytic activity and stability as oxygen reduction electrocatalysts'. *Journal of the American Chemical Society*, 136: (2014), 11687–11697.
73. S. A. Ekanayake, H. Mai, D. Chen and R. A. Caruso, 'Recent advances in synthesis and application of Magnéli phase titanium oxides for energy storage and environmental remediation'. *Chemical Science*, 16: (2025), 2980–3018.
74. Y. H. Li, P. F. Liu, L. F. Pan et al., 'Local atomic structure modulations activate metal oxide as electrocatalyst for hydrogen evolution in acidic water'. *Nature Communications*, 6: (2015), 8064.
75. M. Sundberg, N. Zakharov, I. Zibrov et al., 'Two high-pressure tungsten oxide structures of W_3O_8 stoichiometry deduced from high-resolution electron microscopy images'. *Structural Science*, 49: (1993), 951–958.
76. G. Frey, A. Rothschild, J. Sloan et al., 'Investigations of nonstoichiometric tungsten oxide nanoparticles'. *Journal of Solid State Chemistry*, 162: (2001), 300–314.
77. M. Gerosa, C. Di Valentin, G. Onida, C. E. Bottani and G. Pacchioni, 'Anisotropic effects of oxygen vacancies on electrochromic properties and conductivity of γ-monoclinic WO_3'. *Journal of Physical Chemistry C*, 120: (2016), 11716–11726.
78. M. Gillet, C. Lemire, E. Gillet and K. Aguir, 'The role of surface oxygen vacancies upon WO_3 conductivity'. *Surface Science*, 532: (2003), 519–525.
79. K. W. Böer and U. W. Pohl, *Semiconductor Physics* (Springer, Cham, Switzerland, 2023), pp. 595–648.
80. X. Zhang, L. Gong, K. Liu et al., 'Tungsten oxide nanowires grown on carbon cloth as a flexible cold cathode'. *Advanced Materials*, 22: (2010), 5292–5296.
81. Y. Li, Y. Bando and D. Golberg, 'Quasi-aligned single-crystalline $W_{18}O_{49}$ nanotubes and nanowires'. *Advanced Materials*, 15: (2003), 1294–1296.
82. F. Böttger-Hiller, R. Lungwitz, A. Seifert et al., 'Nanoscale tungsten trioxide synthesized by in situ twin polymerization'. *Angewandte Chemie International Edition*, 48: (2009), 8878–8881.
83. Q. Liu, F. Wang, H. Lin et al., 'Surface oxygen vacancy and defect engineering of WO_3 for improved visible light photocatalytic performance'. *Catalysis Science & Technology*, 8: (2018), 4399–4406.
84. W. Zhou, X. Wang, F. Lin et al., 'Visible-light-driven oxidation of Benzene to Phenol with O_2 over photoinduced oxygen-vacancy-rich WO_3'. *Angewandte Chemie International Edition*, 137: (2025), e202417703.
85. M. Shen, Y. Ye, M. Wang et al., 'Engineering the atomic configurations of surface-active sites for retuning the photoreduction CO_2 selectivity'. *ACS Catalysis*, 14: (2024), 15908–15915.
86. H. Li, J. Zhao, L. Luo, J. Du and J. Zeng, 'Symmetry-breaking sites for activating linear carbon dioxide molecules'. *Accounts of Chemical Research*, 54: (2021), 1454–1464.
87. W. Bollmann, *Crystal Defects and Crystalline Interfaces* (Springer Science & Business Media, Berlin, Heidelberg, Germany, 2012).
88. S. Ida, N. Kim, E. Ertekin, S. Takenaka and T. Ishihara, 'Photocatalytic reaction centers in two-dimensional titanium oxide crystals'. *Journal of the American Chemical Society*, 137: (2015), 239–244.
89. P. Ren, M. Song, J. Lee et al., 'Edge dislocations induce improved photocatalytic efficiency of colored TiO_2'. *Advanced Materials Interfaces*, 6: (2019), 1901121.
90. M. Liu, D. Jing, Z. Zhou and L. Guo, 'Twin-induced one-dimensional homojunctions yield high quantum efficiency for solar hydrogen generation'. *Nature Communications*, 4: (2013), 2278.
91. R. Rousseau, V.-A. Glezakou and A. Selloni, 'Theoretical insights into the surface physics and chemistry of redox-active oxides'. *Nature Reviews Materials*, 5: (2020), 460–475.
92. Z. Yu, D. Yu, X. Wang et al., 'Photoinduced formation of oxygen vacancies on Mo-incorporated WO_3 for direct oxidation of benzene to phenol by air'. *Journal of the American Chemical Society*, 147: (2025), 13885–13892.
93. H. Zhang, Y. Wang, S. Zuo et al., 'Isolated cobalt centers on $W_{18}O_{49}$ nanowires perform as a reaction switch for efficient CO_2 photoreduction'. *Journal of the American Chemical Society*, 143: (2021), 2173–2177.
94. N. Zhang, A. Jalil, D. Wu et al., 'Refining defect states in $W_{18}O_{49}$ by Mo doping: a strategy for tuning N_2 activation towards solar-driven nitrogen fixation'. *Journal of the American Chemical Society*, 140: (2018), 9434–9443.
95. J. Meng, Q. Lin, T. Chen et al., 'Oxygen vacancy regulation on tungsten oxides with specific exposed facets for enhanced visible-light-driven photocatalytic oxidation'. *Nanoscale*, 10: (2018), 2908–2915.
96. Z. Yang, J. Wang, J. Wang et al., '2D WO_{3-x} nanosheet with rich oxygen vacancies for efficient visible-light-driven photocatalytic nitrogen fixation'. *Langmuir*, 38: (2022), 1178–1187.
97. J. Liu, X. Sun, K. Lin et al., 'Optimizing schottky rectifying effect in PtCu/WO_x heterojunctions to accelerate oxygen reduction kinetics'. *Nano Research*, 18: (2025), 94908088.
98. Y. Shi, Z. Wang, Y. Song, J. C. Yu and L. Wu, 'Designing efficient 2D photocatalysts through coordination activation mediated surface engineering'. *ChemCatChem*, 16: (2024), e202401037.

Downloaded from https://www.cambridge.org/core. 18 Nov 2026 at 09:38:25, subject to the Cambridge Core terms of use.

99. M. Sachs, J.-S. Park, E. Pastor et al., 'Effect of oxygen deficiency on the excited state kinetics of WO_3 and implications for photocatalysis'. *Chemical Science*, 10: (2019), 5667–5677.
100. Y. Li, Z. Tang, J. Zhang and Z. Zhang, 'Defect engineering of air-treated WO_3 and its enhanced visible-light-driven photocatalytic and electrochemical performance'. *Journal of Physical Chemistry C*, 120: (2016), 9750–9763.
101. J. Meng, Z. Lan, I. E. Castelli and K. Zheng, 'Atomic-scale observation of oxygen vacancy-induced step reconstruction in WO_3'. *Journal of Physical Chemistry C*, 125: (2021), 8456–8460.
102. J. Wang, K. Liu, W. Liao et al., 'Metal vacancies in semiconductor oxides enhance hole mobility for efficient photoelectrochemical water splitting'. *Nature Catalysis*, 8: (2025), 229–238.
103. Y. Wang, T. Wang, H. Arandiyan et al., 'Advancing catalysts by stacking fault defects for enhanced hydrogen production: a review'. *Advanced Materials*, 36: (2024), 2313378.
104. F. V. Mascaró, M. T. Koper and M. J. Rost, 'Step bunching instability and its effects in electrocatalysis on platinum surfaces'. *Nature Catalysis*, 7: (2024), 1165–1172.
105. G. Liu, A. J. Shih, H. Deng et al., 'Site-specific reactivity of stepped Pt surfaces driven by stress release'. *Nature*, 626: (2024), 1005–1010.
106. A. Mahmood, H. Lin, N. Xie and X. Wang, 'Surface confinement etching and polarization matter: a new approach to prepare ultrathin PtAgCo nanosheets for hydrogen-evolution reactions'. *Chemistry of Materials*, 29: (2017), 6329–6335.
107. H. Arandiyan, S. S. Mofarah, C. C. Sorrell et al., 'Defect engineering of oxide perovskites for catalysis and energy storage: synthesis of chemistry and materials science'. *Chemical Society Reviews*, 50: (2021), 10116–10211.
108. S. Y. Yi, E. Choi, H. Y. Jang et al., 'Insight into defect engineering of atomically dispersed iron electrocatalysts for high-performance proton exchange membrane fuel cell'. *Advanced Materials*, 35: (2023), 2302666.
109. C. Páez, A. Pereira, J. Rodrigues and N. Peres, 'Electronic transport across linear defects in graphene'. *Physical Review B*, 92: (2015), 045426.
110. P. Schweizer, C. Dolle and E. Spiecker, '*In situ* manipulation and switching of dislocations in bilayer graphene'. *Science Advances*, 4: (2018), eaat4712.
111. Y. Sun, Q. Liu, S. Gao et al., 'Pits confined in ultrathin cerium (IV) oxide for studying catalytic centers in carbon monoxide oxidation'. *Nature Communications*, 4: (2013), 2899.
112. Y. Li, R. Jin, Y. Xing et al., 'Macroscopic foam-like holey ultrathin g-C_3N_4 nanosheets for drastic improvement of visible-light photocatalytic activity'. *Advanced Energy Materials*, 6: (2016), 1601273.
113. L. Li, P. A. Salvador and G. S. Rohrer, 'Photocatalysts with internal electric fields'. *Nanoscale*, 6: (2014), 24–42.
114. Y. Liu, L. Liang, C. Xiao et al., 'Promoting photogenerated holes utilization in pore-rich WO_3 ultrathin nanosheets for efficient oxygen-evolving photoanode'. *Advanced Energy Materials*, 6: (2016), 1600437.
115. H. Zhao, F. Pan and Y. Li, 'A review on the effects of TiO_2 surface point defects on CO_2 photoreduction with H_2O'. *J. Materiomics*, 3: (2017), 17–32.
116. Y. Liu, M. Cheng, Z. He et al., 'Pothole-rich ultrathin WO_3 nanosheets that trigger N≡ N bond activation of nitrogen for direct nitrate photosynthesis'. *Angewandte Chemie International Edition*, 58: (2019), 731–735.
117. D. Chen, L. Gao, A. Yasumori, K. Kuroda and Y. Sugahara, 'Size-and shape-controlled conversion of tungstate-based inorganic-organic hybrid belts to WO_3 nanoplates with high specific surface areas'. *Small*, 4: (2008), 1813–1822.
118. G. Liu, J. Han, X. Zhou et al., 'Enhancement of visible-light-driven O_2 evolution from water oxidation on WO_3 treated with hydrogen'. *Journal of Catalysis*, 307: (2013), 148–152.
119. N. Zhang, X. Li, H. Ye et al., 'O oxide defect engineering enables to couple solar energy into oxygen activation'. *Journal of the American Chemical Society*, 138: (2016), 8928–8935.

Downloaded from https://www.cambridge.org/core. 18 Nov 2026 at 09:38:25, subject to the Cambridge Core terms of use.